AIAA SciTech Forum
January 3-7, 2022, San Diego, CA & Virtual
AIAA SCITECH 2022 Forum

10.2514/6.2022-1929

Aerodynamic Verification and Validation of SUAVE

Emilio Botero*, Matthew Clarke†, Racheal Erhard†, Jordan Smart†, and Juan J. Alonso‡
Stanford University, Stanford, CA 94305, USA

Aaron Blaufox§
Exosonic, Los Angeles, CA 90020, USA

SUAVE, as a conceptual-level aircraft design tool, must reliably produce aerodynamic data for new vehicle designs. To ensure that SUAVE can continue to produce accurate data, a series of studies is conducted to examine the behavior of new aerodynamic analyses. These studies helped serve as both verification and validation of SUAVE's software base. Several common aerodynamic models were used, including the NASA Common Research Model, the NASA X-57 Maxwell, PROWIM, and the Onera M6 as well as two simple computational models used for verification. A detailed comparison of SUAVE to both computational and experimental results is shown herein. The goal of this study is not only to provide confidence to users, but also to demonstrate new aerodynamic methods and best practices.

Nomenclature

AoA	=	aircraft angle of attack
b	=	wing span
C_D	=	coefficient of drag
C_L	=	coefficient of lift
C_M	=	coefficient of pitching moment
C_N	=	coefficient of yawing moment
C_P	=	surface coefficient of pressure
C_R	=	coefficient of rolling moment
C_Y	=	coefficient of side force
ΔC_P	=	differential surface pressure $(C_{P,lower} - C_{P,upper})$
S	=	wing area

I. Introduction

SUAVE, since its inception has been built on a strong belief in verification and validation (V&V) of code. Certainly, V&V is important in any analysis software. However, an extreme emphasis on developing accurate and tested analyses was taken from the beginnings of SUAVE and continues through this day.

Unconventional aerospace vehicle designs break the assumptions of traditional configurations. Credibly designing these unconventional vehicles requires the designer to have the utmost faith in their software tools to ensure these new vehicle designs are truly superior. Traditional design codes provide exceptionally accurate results for conventional aircraft designs. Such codes have various assumptions and empirical corrections that are specifically tuned to pre-existing aircraft with standard configurations. However, these assumptions fail to capture the intricacies of unconventional vehicles, of which there has been significant recent interest. Hence, SUAVE was born out of this need for analyses that moved away from correlative methods and towards physics-based approaches that require minimal, if any, parameter adjustments.

In the earliest days of SUAVE, the codebase was heavily verified against existing conceptual design codes to verify performance [1]. In the years since, SUAVE has grown in many ways. As a multifidelity code [2, 3] it has expanded the

*Postdoctoral Scholar, Department of Aeronautics and Astronautics.
†Graduate Student, Department of Aeronautics and Astronautics, AIAA Student Member.
‡Vance D. and Arlene C. Coffman Professor, Department of Aeronautics and Astronautics, AIAA Fellow.
§Performance Engineer

levels of fidelities provided to the user. Additionally, the “low fidelity" analyses have also increased in capabilities. In truth, the “low fidelity" methods of SUAVE are nothing like the simple hand calculations of the first beta releases many years ago. These new “low fidelity" methods are indeed quite sophisticated, yet with modern programming methods they can be executed very quickly on arbitrary aircraft configurations.

This publication seeks to show how SUAVE has grown through its many releases to provide the same strong V&V while growing its capabilities to credibly analyze unconventional vehicles. We highlight several new validation test cases using SUAVE’s low fidelity methods. In highlighting these cases here we can both provide confidence to users as well as provide new methods to the broader aerospace community.

II. New Methods

A. Aerodynamic Analyses

SUAVE’s initial aerodynamics models were built off of a version of Weissinger’s Lifting Line model [4]. Although this method is very computationally efficient, it had many drawbacks. First, the method as described had no native Mach number effects, requiring SUAVE at the time to impose a Prandtl-Glauert compressibility correction. Second, although this method can account for swept wings (unlike traditional lifting line methods), it does not account for chordwise variations in pressure. These limitations affected many of the more complex configurations SUAVE users were seeking to analyze, such as coupled wings with propellers or supersonic transport aircraft. Thus, SUAVE’s Weissinger model was replaced with a Vortex Lattice Method (VLM) as the standard level of aerodynamic analysis.

The first iterations of this VLM were based on subsonic methods. After continuously adding corrections to an original formulation of this VLM method, it was decided to port the original VORLAX Fortran code by Miranda et. al [5] to Python3. This provides native support for both subsonic and supersonic results in a unified set of analyses. This port of VORLAX gave the SUAVE developers further confidence in the results, as they match VORLAX exactly while eliminating the antiquated coding styles. This part of the process of exactly matching VORLAX fulfills the verification requirement but falls short of the validation requirement of V&V. Porting VORLAX into Python3 from Fortran, counter-intuitively sped up the computation of the VLM code. This speedup was because the formulation in SUAVE has no "DO" or "GO TO" statements and does not require any convergence loops. Instead, any equation is only executed once regardless of the number of angles of attack or Mach numbers, in a vectorized manner. Furthermore, this formulation expanded the capabilities of SUAVE to handle sideslip angles and the stability effects of acceleration rates.

While the core equations from VORLAX are ported to SUAVE, other aspects of the code start anew. The discretization methods were started from scratch, allowing for more complex geometries. Now wings of all kinds, fuselages, nacelles, and even control surfaces can be added arbitrarily to the configurations. Wings, fuselages, and nacelles can be made of complex segmented shapes that carry over to the VLM panelization. The discretization methods adjust to account for breaks and discontinuities in the geometry. The inclusion of control surfaces adds new capabilities for future versions of SUAVE. The new discretization methods also allow for easier computation of asymmetrical vehicle configurations. Each vortex filament is prescribed its own axis system. The results are solved in the vortex frame and transformed back into the vehicle frame. It was found that this eliminated edge cases found in VORLAX with unusual geometries. The solution process is modernized with the vortex strengths solved via a matrix solve using SciPy.

Some of the results presented in this paper include additional drag from build-up techniques as necessary. These techniques add additional contributors to drag beyond the inviscid drag from the VLM [1]. The components of drag may include viscous drag build-ups, compressibility drag due to thickness, wave drag, trim drag, and conceptual level design excrescence drag. For verification and validation, it is insufficient to only produce correct inviscid results; the combination of the VLM results with the drag build-up must be considered. The drag build-up relies on information from the VLM. Therefore a small error in the inviscid lift or drag can have an increased error in later drag analyses.

III. Test Cases

To showcase SUAVE’s applicability to predicting the aerodynamic performance of a wide range of aircraft, several test vehicles familiar to the aerospace community were selected as validation cases. Many of the test cases have a wealth of data including experimental and computational results, including the NASA Common Research Model, the NASA X57 Maxwell, the Onera M6, and the PROWIM experimental wing. Where experimental data is unavailable, computational comparisons are made for verification to other software methods. The results of this section were executed using SUAVE 2.5 [6]. Except as mentioned specifically, the results represent the behavior of SUAVE with the parameters as defaulted. No tuning of parameters or adjustments were made to SUAVE for the preparation of the presented results.

A. Common Research Model

The NASA Common Research Model (CRM) began as a way to validate and guide CFD research [7, 8]. The original High Speed CRM was used in the fourth AIAA CFD Drag Prediction Workshop in 2009. However, since then the CRM has expanded in use and spawned several variants. This use has created a wealth of both experimental and computational published studies with data. After some time, it was discovered that while the experimental data was self-consistent and the CFD data was as well, the experimental data was not matching the CFD results. This lead to further examination culminating in the discovery that the experimental results had issues with the setup [9]. The consequence of this discovery was an adjusted CRM with twisted wing profiles. Thus, there are two High Speed CRM geometries. While simple at first glance, the CRM geometry is more complex than one would expect. The airfoil sections and twists of the main wing vary tremendously throughout the span. This coupled with the definition of the two High Speed CRM models influenced how the vehicles were input into SUAVE. The original CRM is well defined in the work by Vassberg [7]. This original CRM was directly modeled using SUAVE's native format. However, there is no simple geometric representation of the Twisted CRM. The Twisted CRM required importation into OpenVSP via the STP files distributed with the sixth AIAA CFD Drag Prediction Workshop [10]. An example of importation can be seen in Figure 1a. The OpenVSP model was created using the Fit Model tool to create a parametric version of the CRM that could be imported into SUAVE.

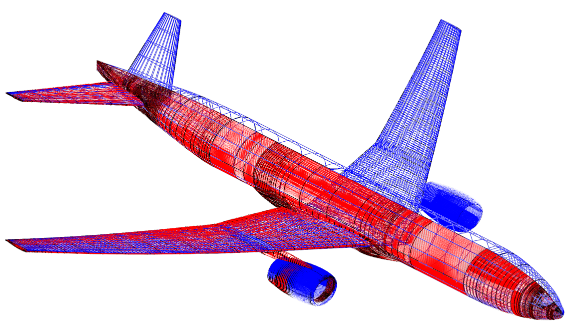

(a) NASA CRM Importation with OpenVSP

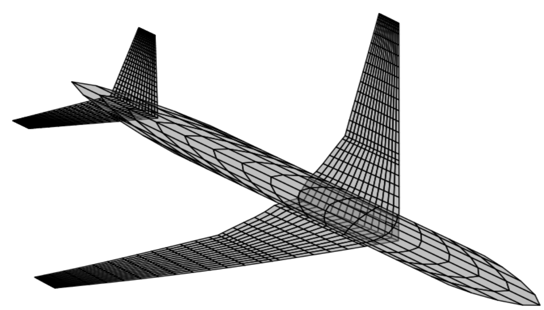

(b) SUAVE CRM VLM Panelization

Fig. 1 Common Reference Model.

For the examples shown here, the simple Wing/Body/Tail Twisted CRM with a 0-degree tail angle is used. With the Twisted CRM now imported into SUAVE via OpenVSP, the VLM discretized the model into a zero-thickness representation. The fine discretization of the parametrization of the geometry consequently required a fine grid for the VLM. An image of the VLM can be seen in Figure 1b. This VLM has the dimensions, sweeps, twists, and mean camber line of the airfoil sections. The discretization of each wing panel in this VLM model is 50 panels spanwise per half span and 30 chordwise. To better illustrate the grid, Figure 1b has half that number used. Fuselage discretization is independent of wing panelization. The fuselage has 16 panels lengthwise and 4 in the spanwise direction. The discretization is cosine spaced in the spanwise direction and linear in the chordwise direction. The trailing vortices of the VLM, those which extend to infinity, follow the same angle as the last chordwise panel. Thus, the trailing vortices do not kink at the trailing edge of the wings. The test cases for this study are those from Rivers et. al [11]. This includes the experimental data from the National Transonic Facility (NTF). The specific run that is used for comparison to the experimental case is from test run 92. This run is at a Reynolds number of 5 million for the reference chord and a Mach number of 0.85. The corresponding CFD data is from the publication by Rivers documenting the Twisted CRM [9] using USM3D. This CFD data as presented does not have the adjustments with the support system or arc sector. The reason to present this specific CFD data is that SUAVE cannot easily be adjusted for this experimental setup.

Presented here is the coefficient of lift versus angle of attack in Figure 2a, followed by the coefficient of drag in Figure 2b, and finally coefficient of moment in Figure 2c. The coefficient of lift shows a flattening of the lift curve slope after three degrees angle of attack. After this point, sonic effects on the wing begin to affect the performance. These Mach effects on lift cannot be simply captured by a flat VLM geometry as they are dependent on the thickness. The drag buildups in SUAVE do address the compressibility effects due to thickness, but not at a fine level to address the nuances of the airfoil profiles. After examining the results in Figure 2b, we see that the drag values are very close to what would be expected for values of the CRM's design lift coefficient of 0.5. However, the overall shape of the drag polar does not follow well at the extremes. Finally, the slope of the moment coefficient roughly matches that of both the experimental data and the USM3D results, but the intercept is slightly off. Some of the error in the moment coefficient may be due to a stack up of errors in importing the model. However, given that the error is similar to that of the CFD data this result is of no concern.

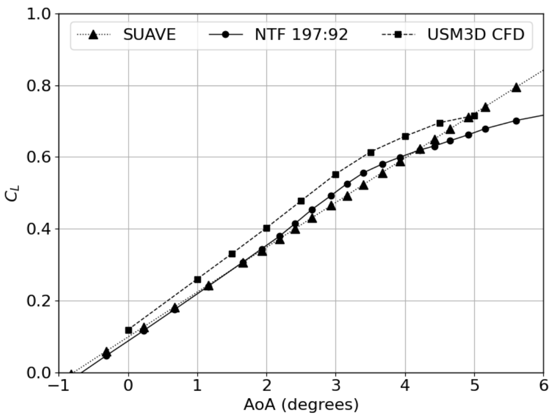

(a) Coefficient of Lift vs Angle of Attack

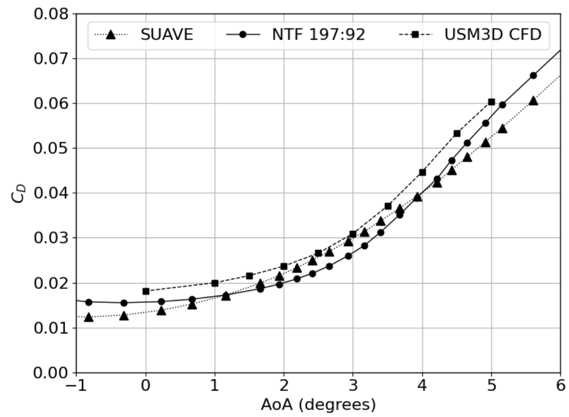

(b) Coefficient of Drag vs Angle of Attack

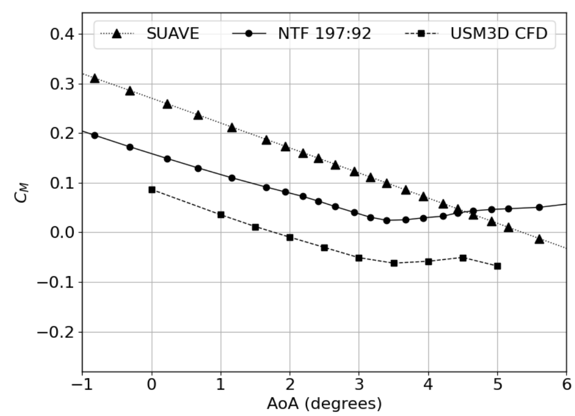

(c) Coefficient of Moment vs Angle of Attack

Fig. 2 Twisted CRM Wing/Tail/Fuselage

Predicting the performance of a vehicle at transonic Mach numbers is notoriously difficult, hence the AIAA Drag Prediction Workshop series. However, SUAVE has shown that for a conceptual level tool it does provide very reasonable results to both the USM3D CFD results as well as wind tunnel data while being much more computationally efficient.

B. Subsonic Commuter Aircraft Validation: NASA X-57 Maxwell

The second validation study of the newly implemented VLM was that of a general aircraft that operates around cruise speeds of 135-175 mph at a service ceiling around 15,000 ft and is designed to service short-range regional flights. The specific model used in this study was inspired by NASA's X-57 Maxwell experimental aircraft. This aircraft is a high-wing, all-electric technical demonstrator designed to carry a maximum of four passengers. The Maxwell itself is developed by modifying a Tecnam P2006T aircraft with an electric powertrain. Two sets of results are presented below. The first is the Modification-II variant which has one propulsor mounted on each wing around the mid-span and the second is the Modification-III variant of NASA's X-57 Maxwell that possesses a higher aspect ratio wing with wing-tip mounted propulsors and high-lift nacelles for the integration of a distributed electric propulsion powertrain system. In the VLM analysis, the vertical section of the fuselage is omitted in the VLM panelization while control surface discretization for the second set of comparisons is included as their effectiveness is studied.

1. X-57 Modification-II

In this sub-case, the performance of SUAVE's Fidelity Zero (VLM with Mach and drag corrections) to predict aerodynamic performance is measured against experimental data obtained from wind tunnel experiments conducted by Nicolosi et. al [12]. In this test campaign, a 1:6.5 scale wooden model was used and two variants of the aircraft were analyzed – a clean configuration (wing and body only) and a configuration with wing-mounted nacelles – to evaluate the effect of the engines on aircraft aerodynamics. Here, we present the results of the clean configuration. Similar to the experiments, a NACA 63-412 airfoil is used to model the wing sections. Properties of the computational domain were also modified to emulate similar experimental test conditions with Reynolds numbers around 0.6×10^6. Moreover, as the VLM is inherently an inviscid prediction tool, it is incapable of modeling flow separation at high angles of attack. As a result, high angles of attack were not examined. Table 1 summarizes the high-level parametrization of the Modification-II (Mod.-II) as well as the test conditions used for the purposes of reproducing the findings presented.

Table 1 Mod.-II Simulation Parameters.

Parameter	Value
Vehicle Geometry	
Reference Area (m^2)	14.76
Center of gravity [x,y,x] (m)	[3.23,0,0.77]
Mean Aerodynamic Chord (m)	1.19
Span(m)	11.4
Test Conditions	
Case 1	
Angle of attack sweep (°)	-2 – 12
Mach Number	0.3
Reynolds Number	0.6×10^6

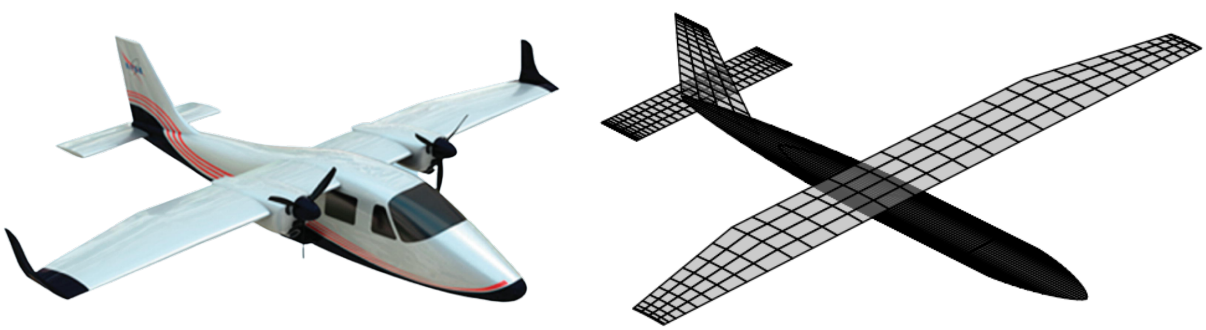

(a) X-57 Mod.-II Rendering **(b) X-57 Mod.-II VLM Panelization.**

Fig. 3 X-57 Modification II Aircraft.

Generally speaking, great agreement was found between SUAVE's aerodynamic analysis routine and the experimental data. In the case of the lift curve slope in Figure 4a, the computational predictions fall within 5% of wind tunnel measurements up to an angle of attack of 7°. After which, an expected overprediction of the lift coefficient is observed. The VLM however slightly underpredicts the zero-lift angle of attack as shown in the plot. The linearized drag polar in Figure 4b on the other hand highlights a more significant discrepancy between the measured and predicted drag, particularly at low angles of attack. Between a lift coefficient of 0 (AoA = -2.5°) and a lift coefficient of 0.7 (AoA = 7.1°), there is an underprediction of drag by as much as 100 drag counts when the aircraft is pitched nose-down. Predictions within the region of the curve where this aircraft is expected to operate are closer to the experimental data and do point to the VLM being suitable for providing more than sufficient estimates for aerodynamic loads in a full mission.

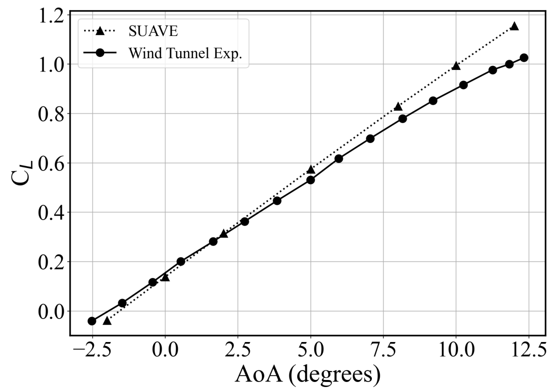

(a) Lift coefficient vs angle of attack.

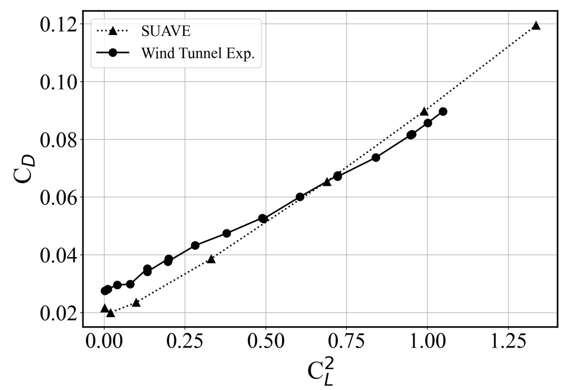

(b) Linearized drag polar.

Fig. 4 X-57 Modification-II Validation.

2. X-57 Modification-III

The second study regarding the external aerodynamics of an unpowered X-57 Modification-III (Mod.-III) configuration was carried through a comparison with computational fluid dynamics (CFD) results obtained from Yoo and Duensing [13]. In their study they use two Reynolds-averaged Navier-Stokes (RANS) flow solvers: STAR-CCM+, a commercial code, and Launch Ascent Vehicle Aerodynamic (LAVA), which is a code developed and maintained by NASA Ames Research Center. In this paper, however, only the results of STAR-CCM+ which solves the RANS equation in finite-volume, cell-centered formulation are provided. Using this commercial code, the inviscid fluxes were discretized using the second-order Roe flux-difference splitting scheme. Additional information about the solver, turbulence model and preconditioning can be found in the reference. Here we assess the performance of the SUAVE's VLM for two flap-deflection angles, cruise (0°) and takeoff (10°). The aircraft itself is designed to be a configuration with a blown wing, and has a higher aspect ratio with nacelles distributed along the wingspan. Those at the wingtips are for mounting larger propellers for efficient cruises while the smaller ones inboard are for high-lift flight regimes such as takeoff and cruise. Again, the high-level geometric parameters and flight conditions used in the simulations are documented in Table 2.

Table 2 Mod.-III Simulation Parameters.

Parameter	Value
Vehicle Geometry	
Reference Area (m^2)	6.13
Center of gravity [x,y,x] (m)	[3.35,0,0.34]
Mean Aerodynamic Chord (m)	0.65
Span(m)	9.64
Test Conditions	
Case 1	
Angle of attack sweep (°)	-2 – 18
Mach Number	0.233
Reynolds Number	1.32×10^6
Flap Deflection (°)	0
Case 2	
Angle of attack range (°)	-2 – 18
Mach Number	0.233
Reynolds Number	1.32×10^6
Flap Deflection (°)	10

Similar to the twin-engine case, there is a close agreement of the predicted lift coefficient of both the undeflected and deflected flap cases up to about 8° angle of attack where flow separation dominates, particularly on the upper surface of the wing. This separation is computed by the CFD solver and is seen in Figure 6a by the gradual attenuation of lift as the angle of attack increases. There is also an underprediction of total drag at low angles of attack, more than likely attributed to nacelles on the wing that have a non-negligible contribution to the profile drag of the aircraft. On the other hand, the higher predicted drag coefficient in Figure 6b past an angle of attack of 10° is believed to be a result of the overprediction of lift-induced drag. These findings highlight areas in which the code can be improved, notably with the inclusion of a stall model that corrects inviscid aerodynamic predictions and an improvement of profile drag estimates of non-lifting bodies such as boom, nacelles and fixed landing gear systems.

Finally, concerning pitching moment in Figure 6c, we observe less than 10% difference in most of the angle of attack sweep up to an angle of attack of 16°, above which the computation predictions diverge. This was deemed acceptable for a mid-fidelity method such as a VLM based on potential theory.

(a) X-57 Mod.-III rendering

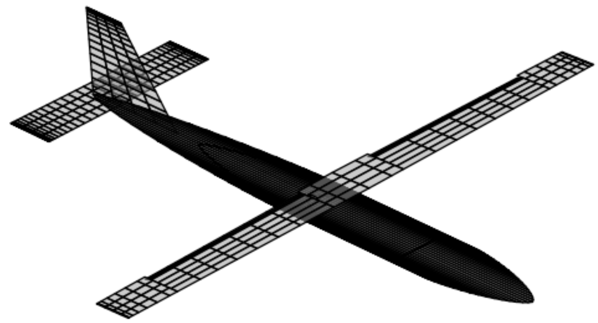

(b) X-57 Mod.-III VLM panelization with deflected flaps.

Fig. 5 X-57 Modification III Aircraft.

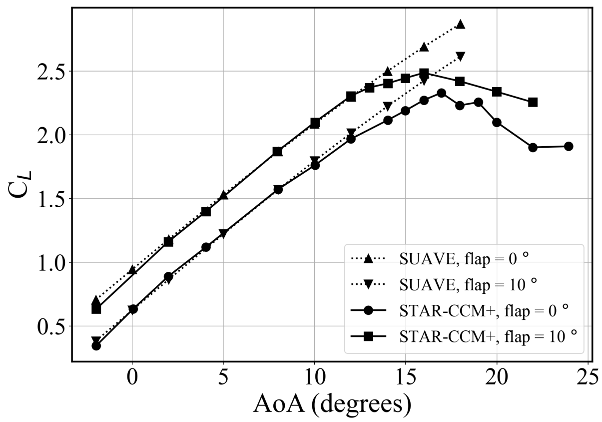

(a) Lift coefficient vs angle of attack.

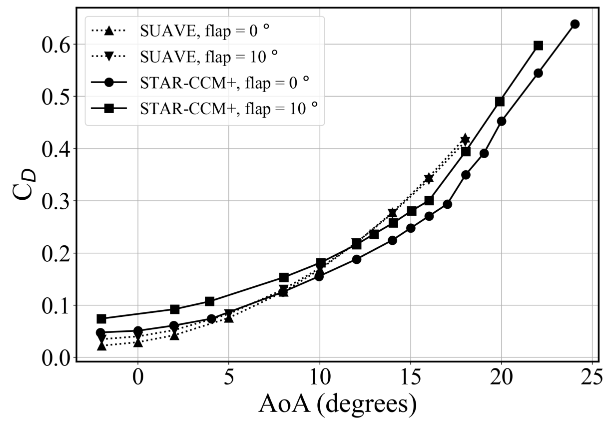

(b) Drag coefficient vs angle of attack.

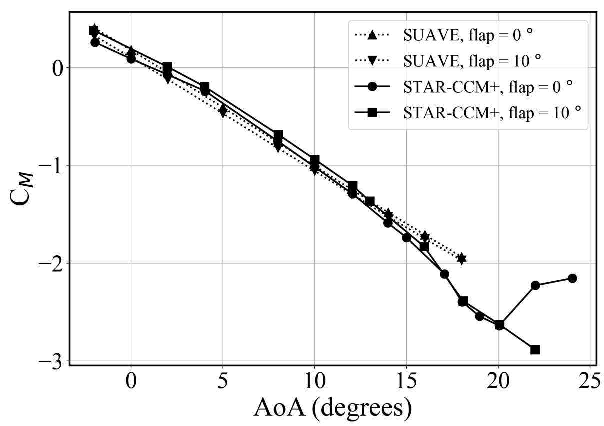

(c) Moment coefficient vs angle of attack.

Fig. 6 X-57 Modification-III Validation.

C. Supersonic Wing Verification

To examine the capabilities of the VLM at supersonic mach numbers a simple verification study was performed. A biconvex "arrow" shaped wing is modeled in SUAVE, PAN AIR, and SU2. This represents three different levels of computational fidelity. This allows for examination of the drag build up beyond the drag captured by the VLM.

A biconvex wing with a 60 degree leading edge sweep was chosen as it represents a basic wing geometry that may be used as a part of a supersonic transport. The parameters of the wing as well as the test conditions are shown in Table 3. All analyses are inviscid, thus Reynolds numbers and the like are excluded.

PAN AIR [14] was chosen as a method as it is a step above SUAVE's baseline fidelity level. The panel method of PAN AIR provides thickness producing volumetric wave drag not captured in an infinitely thin VLM. Although VORLAX has the ability to produce 3D geometrical shell shapes, the discretization capability was not transferred over into SUAVE. PAN AIR excels in low subsonic or pure supersonic flow. The next higher level of fidelity is SU2 CFD [15]. An Euler simulation was performed as inviscid results are preferred for this comparison. The Jameson-Schmidt-Turkel numerical scheme is used for solving. An unstructured mesh with 677,802 elements with multigrid is used, and a maximum CFL of 10 is specified.

In SUAVE, the wing is discretized into 50 chordwise and 50 spanwise elements as seen in Figure 7. The spanwise elements are cosine spaced. To adjust for volumetric wave drag, existing buildups in SUAVE, based on Raymer's methods are used [16]. The volumetric wave drag scaling is set to 1 because of the simple configuration. For the VLM the "SPC" option which modulates leading edge suction is set to 0. This "SPC" value is a typical setting for a supersonic configuration.

Table 3 Biconvex Simulation Parameters

Parameter	Value
Vehicle Geometry	
Reference Area (m^2)	198
Center of gravity [x,y,x] (m)	[4.25,0,0]
Reference Length (m)	17
Span(m)	22
Aspect Ratio	$2.\overline{4}$
Taper Ratio	1/17
Leading Edge Sweep (deg)	60
Test Conditions	
Cases	
Angle of attack sweep (°)	-2 – 6
Mach Numbers	1.4, 1.6, 1.8

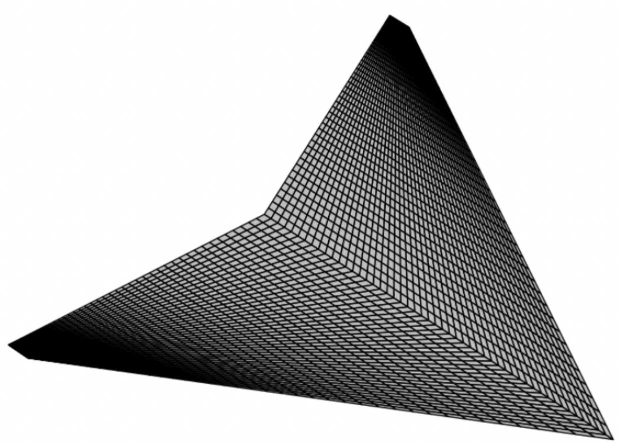

Fig. 7 Biconvex Wing Panelization

The results of the multifidelity supersonic comparison are shown in Figure 8. The general trends of reducing lift with increasing mach numbers is followed by all three methods. However, the slopes vary between all three, and since it is a biconvex airfoil with no twist the intercept is zero. The drag coefficients are plotted against angle of attack. Interestingly SUAVE nearly falls on top of the drag results from PAN AIR, while all three align at a Mach number of 1.6. One important aspect of the drag is the zero lift offset caused by volumetric wave drag for all three analyses is very close. Finally, the moment coefficient is compared against SU2 only. The moment coefficients align at a Mach number of 1.8, but at lower Mach numbers fails to properly match.

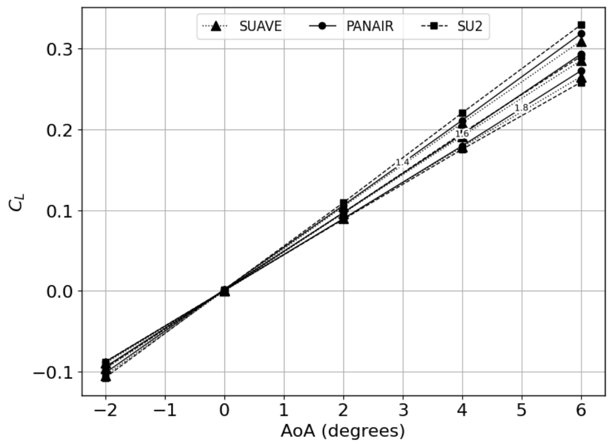

(a) Coefficient of Lift vs Angle of Attack

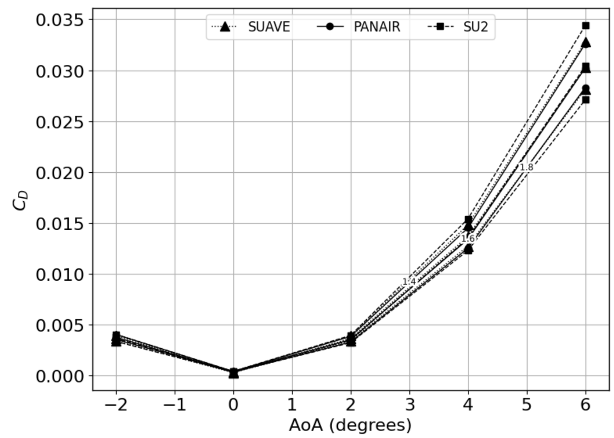

(b) Coefficient of Drag vs Angle of Attack

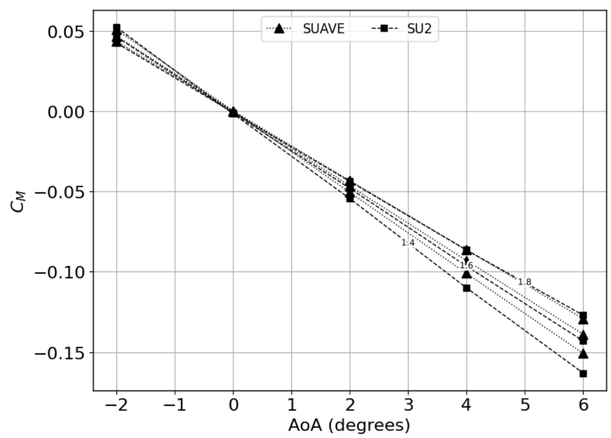

(c) Coefficient of Moment vs Angle of Attack

Fig. 8 Biconvex Wing Results

D. Control Surfaces Verification

One of the new features added to SUAVE was the ability to add control surfaces into the Fidelity Zero aerodynamics analysis. Previously with SUAVE, the only way to include the effects of control surfaces was to interface with Athena Vortex Lattice (AVL) [3, 17]. In this section the results are compared against AVL with identical discretization parameters and flight conditions.

The control surfaces are discretized as separate surfaces independent of the parent wing. The wings are modified to have cutouts to fit the control surfaces, with vortices shifted as necessary. Thus, the chordwise vortices tends to show some bunching either onto the wing or control surfaces. The discretization pattern from the wing in the spanwise direction continues onto the control surfaces. When the control surfaces are not deflected the wing and control surfaces appear as a continuous surface. The example here is of a medium range single aisle airliner, as is used in the SUAVE Tutorials, and seen discretized in Figure 9. The image shows 20 spanwise vortices and 10 chordwise vortices and the all control surfaces deflected. The fuselage is not modeled for comparisons here. For the computational experiments, 40 spanwise vortices and 20 chordwise vortices are used with cosine spacing in the spanwise direction.

An angle of attack sweep is performed with a range of deflection. The ailerons, elevators, and rudder are separately deflected at 0, 15, and 30 degrees. The primary force and or moment contribution is plotted for each surface. Although flaps are modeled in the vehicle, they are not deflected for this comparison. A breakdown of the coefficients is shown in Figure 10. The results for the aileron produce nearly identical coefficients of roll compared to AVL. Both capture a reduction of roll moment with an increase in angle of attack. Similarly, the lift coefficient and pitching moment coefficient overlap nicely with AVL. However, some differences are found for rudder deflections, with SUAVE producing a higher side force and yaw moment coefficient. It is suspected that discretization differences between AVL and SUAVE in the rudder caused these small discrepancies in yaw due to rudder.

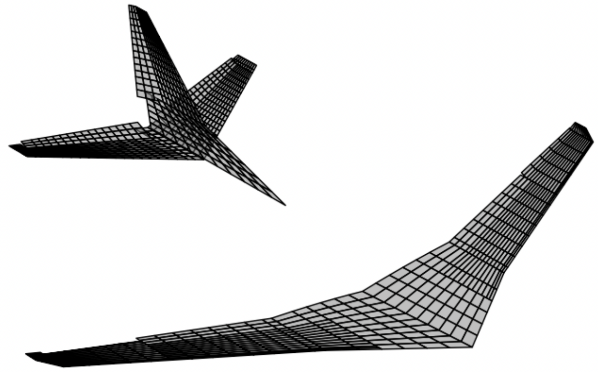

Fig. 9 Medium Range Airliner Panelization

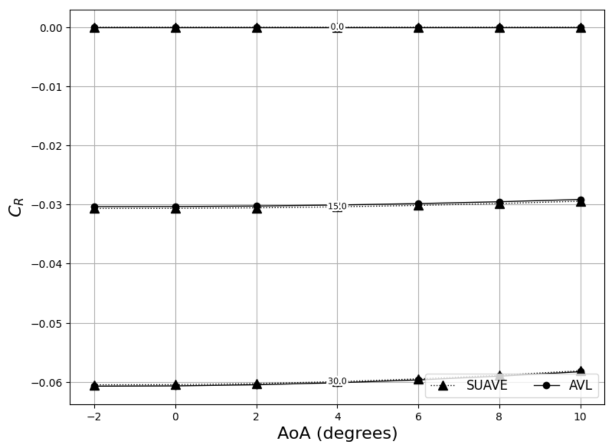

(a) Roll Moment vs Angle of Attack due to Aileron

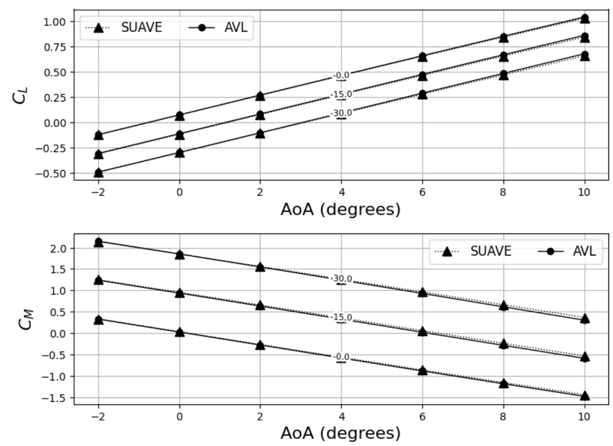

(b) Lift and Pitching Moment vs Angle of Attack due to Elevator

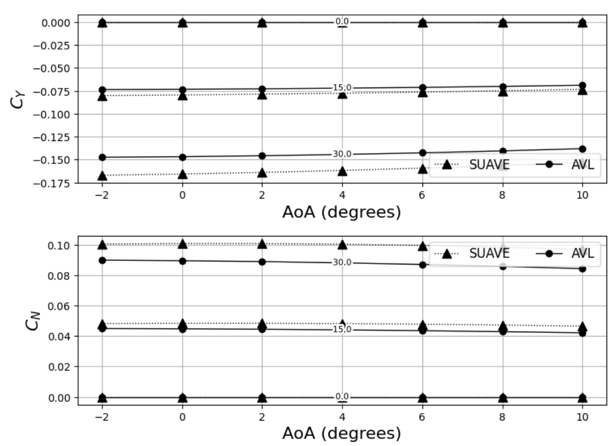

(c) Side Force and Yaw Moment vs Angle of Attack due to Rudder

Fig. 10 Medium Range Airliner with Control Surface Results

E. Validation of Pressure Distribution on PROWIM Experimental Wing

This section evaluates the accuracy of the surface pressure distribution generated by the new VLM in SUAVE against the PROWIM experimental wing [18]. This subsonic straight wing has an aspect ratio of 5.33 and a half span of $0.64m$, with constant chord and NACA 64_2A015 airfoil section. It was developed as a baseline propeller-wing test setup and used to explore the slipstream effect of a tractor-configured propeller over the wing. Validation of the spanwise lift coefficient distribution in the presence of the propeller slipstream has previously been conducted using a combined prescribed vortex wake model with the VLM in SUAVE [19]. For the purpose of this paper, we further demonstrate the accuracy of the VLM in SUAVE against experimental data that was obtained for the clean wing test case. Here we explore the total lift coefficient of the wing over a range of angles of attack, as well as more detailed pressure distributions along the chord at various spanwise locations.

A comparison of the computed and measured lift coefficient versus angle of attack is shown in Figure 11a, with close agreement of the VLM in SUAVE to within 8%. The surface pressure measurements were taken along the upper and lower surfaces of the PROWIM wing at the spanwise locations provided in Table 4, as depicted in Figure 11b. For the conditions provided in Table 4, the differential pressure distributions along the chord at each station are compared to the experimental results in Figure 12. From these results, it is clear that SUAVE performs quite well, very closely matching the experimental pressure difference across the tested locations.

Table 4 PROWIM Simulation Parameters

Parameter	Value
Vehicle Geometry	
Span (m)	1.28
Mean Aerodynamic Chord(m)	0.24
Reference Area	0.3072
Test Conditions	
Case 1	
Dynamic pressure	$1500Pa$
Reynolds Number	0.8×06
Mach Number	0.15
Angle of Attack (°)	0 – 10
Case 2	
Dynamic pressure	$1500Pa$
Reynolds Number	0.8×06
Mach Number	0.15
Angle of Attack (°)	4.2
Spanwise loc.	$[0.1742, 0.3453, 0.5922, 0.8108]$

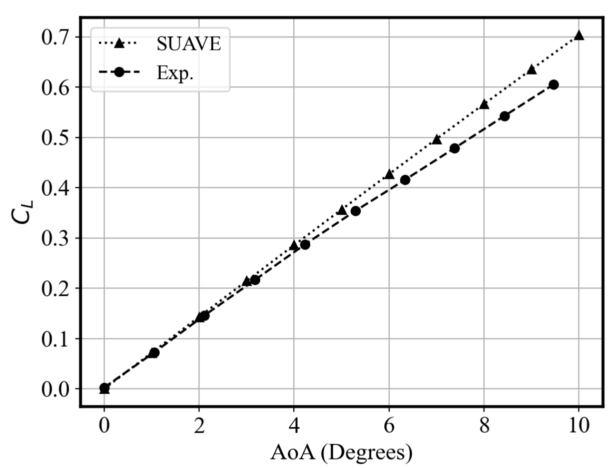

(a) Coefficient of Lift vs. Angle of Attack

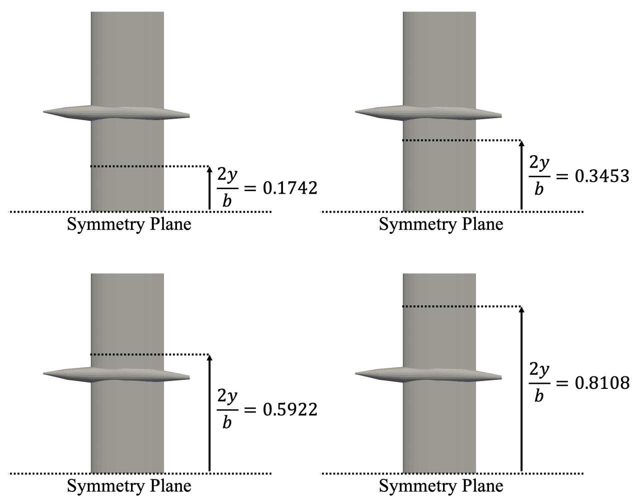

(b) PROWIM wing geometry with spanwise locations of pressure evaluations.

Fig. 11 Prowim Lift and geometry

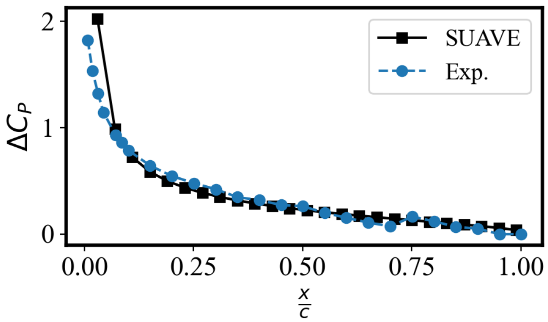

(a) Pressure difference at $2y/b$ = 0.1742.

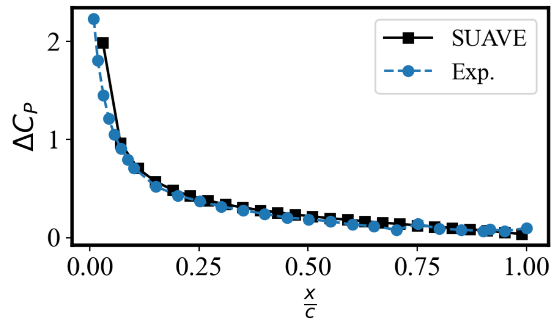

(b) Pressure difference at $2y/b$ = 0.3453.

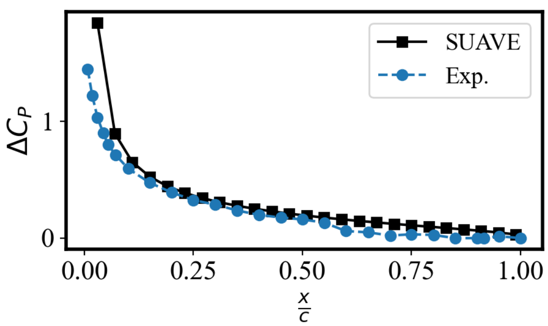

(c) Pressure difference at $2y/b$ = 0.5922.

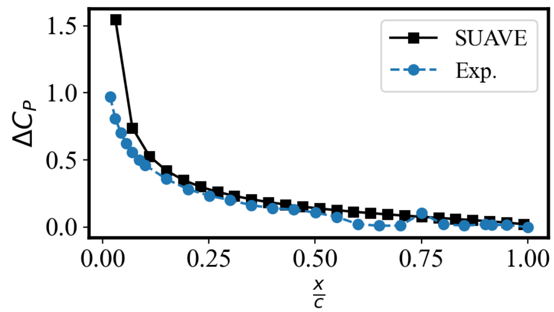

(d) Pressure difference at $2y/b$ = 0.8108.

Fig. 12 Pressure differences

F. Pressure Distribution Comparison on ONERA M6

The ONERA M6 is and was an isolated wing profile developed in the 1970s explicitly for aerodynamic study of transonic flows, rather than for use onboard any particular civilian or military aircraft. As a result, it is purely analytically designed - specified entirely by *a priori* mathematical formulas as opposed to having its profile determined via CAD specification or empirical shaping. This allows the profile to be exactly reproduced within simulation and results compared directly to experimental data without need to account for uncertainty introduced by possible discrepancies between the experimental and simulation models. As such, the M6 has been used extensively in aerodynamic validation studies, including SU2, STAR CCM, Flow360, and others.

Within SUAVE's VLM, the M6 is modeled directly from the parameters provided by the original Schmitt and Charpin report to NATO's Advisory Group for Aerospace Research and Development (AGARD) AR-138.[20] The exact parameters, including the M6's uniform airfoil profile, and the experimental data were retrieved from the NASA Glenn Research Center's archive of the National Program for Applications-Oriented Research in CFD (NPARC).[21] The wing geometric and test conditions are summarized in Table 5.

Table 5 ONERA M6 Simulation Parameters

Parameter	**Value**
Vehicle Geometry	
Span (m)	1.1963
Mean Aerodynamic Chord(m)	0.64607
Leading Edge Sweep (°)	30.0
Trailing Edge Sweep (°)	15.8
Aspect Ratio	3.8
Taper Ration	0.562
Test Conditions	
Mach Number	0.8395
Reynolds Number	11.72E+06
Angle of Attack (°)	3.06
Angle of Sideslip (°)	0.00

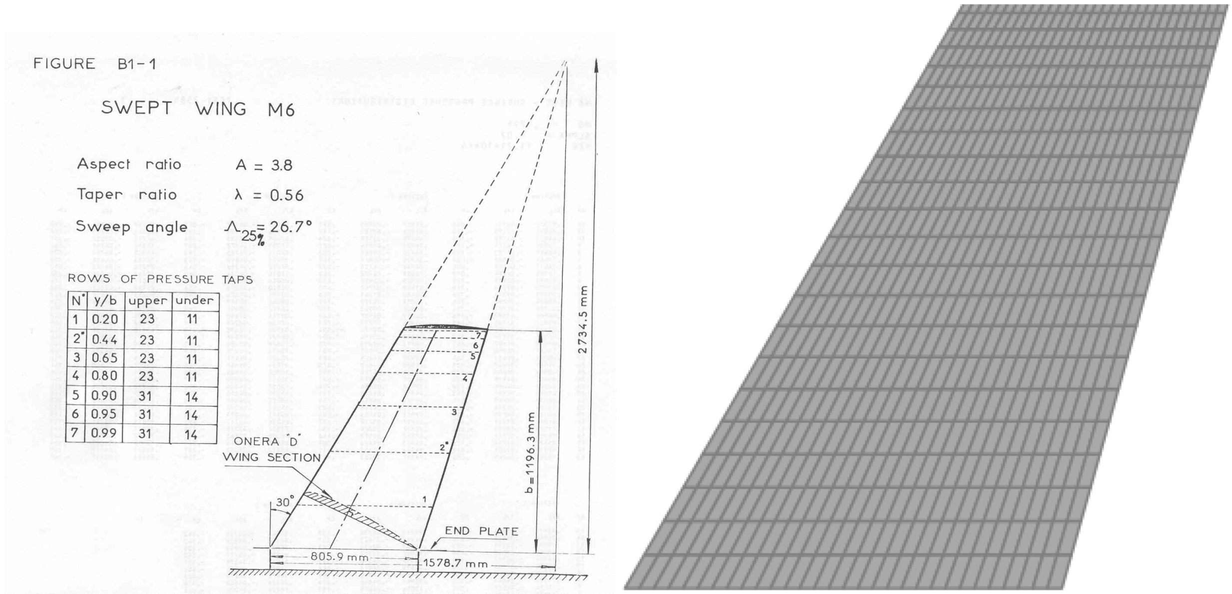

(a) ONERA M6 Specification **(b) ONERA M6 SUAVE VLM Panelizations**

Fig. 13 ONERA M6

The data available from the M6's experimental tests consist of a set of C_p records derived from individual pressure taps on the upper and lower surfaces of the wing at several spanwise station. As SUAVE's VLM calculates ΔC_p as opposed to separate C_p values for the upper and lower surface, the reference values for the M6's upper and lower surfaces are presented along with SUAVE's ΔC_p calculation, and a ΔC_p estimate derived by linearly interpolating between the pressure readings of the lower surface and comparing these interpolated values with the data on the upper surface.

Figure 14 presents data for four separate spanwise locations, at $y/b = 0.20, 0.4, 0.80$, and 0.90. The solid line is SUAVE's VLM ΔC_p calculation, the individual squares and triangles are respectively the lower and upper surface C_p data, and the dashed line is the interpolated ΔC_p of the experimental data.

In general, SUAVE's VLM is able to make good prediction of the ΔC_p near the leading and trailing edges, but in the intermediate range of $0.1 <= x/c <= 0.60$ there are notable discrepancies which increase in magnitude further along the span of the wing.

This discrepancy is most likely due to the formation of overwing shocks, which the VLM cannot explicitly model and account for. This can most clearly be seen in the significant discontinuity in upper surface C_p at the $y/b = 0.90$ station in Figure 14d, with lesser versions notable in the inboard sections.

Though the overall C_L of the M6 does not survive from the original AGARD report, we can compare SUAVE's calculation to results from CFD validated against the same experimental test case. SU2's Euler solver predicts a C_L o approximately 0.285[15], while SUAVE's VLM predicts a C_L of approximately 0.148, resulting from the lower ΔC_p of the VLM's estimate in the pre-shock region. This behavior can be expected to generalize to many transonic cases, and as such where higher fidelity is needed, SUAVE's modules for SU2 or another CFD solver are preferred.

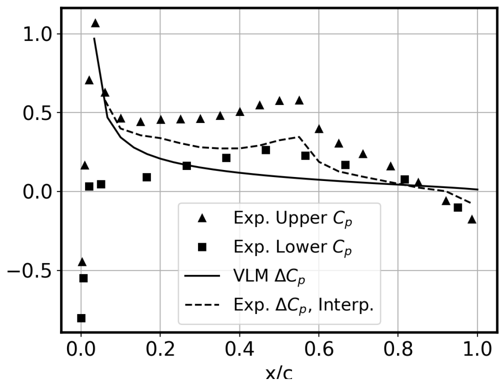

(a) Pressure difference at $y/b = 0.20$**.**

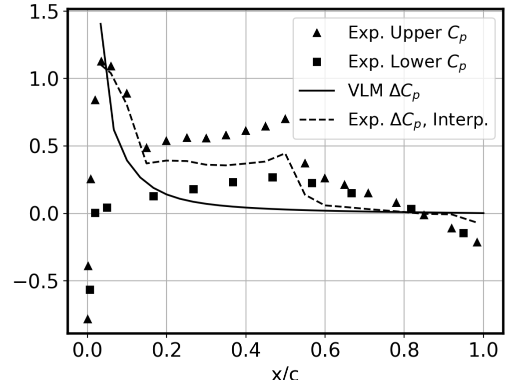

(b) Pressure difference at $y/b = 0.44$**.**

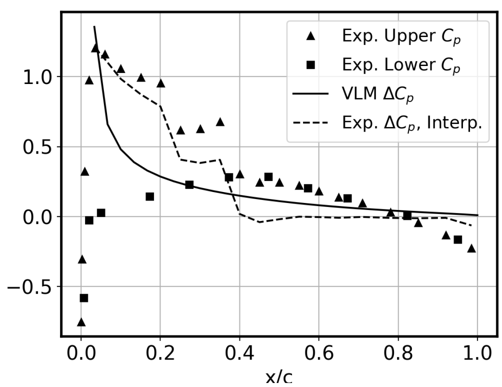

(c) Pressure difference at $y/b = 0.80$**.**

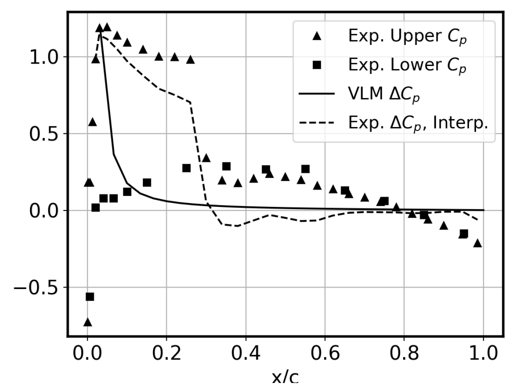

(d) Pressure difference at $y/b = 0.90$**.**

Fig. 14 ONERA M6 C_p **vs SUAVE VLM** ΔC_p**.**

IV. Conclusion

In this work, we have presented new aerodynamics analyses as well as test cases that illustrate the use. The most significant of these new methods is a new Vortex Lattice Method based on the formulation in VORLAX, but with modernized code practices. The aerodynamic analyses were executed on the twisted NASA Common Research Model, NASA X-57 Maxwell in Mod II and III configurations, a supersonic biconvex wing, a medium range airliner, PROWIM, and the Onera M6. All of the results show These results were obtained using a standard release of SUAVE with no tuning beyond the assumptions explicitly mentioned.

The studies here highlight some of the exceptional abilities of SUAVE as well as areas where these analyses underperform. For both pure subsonic and supersonic flight, SUAVE's Fidelity Zero shows excellent agreement to experimental data and high fidelity analyses. Areas of caution are transonic cases with high lift, as SUAVE over-predicts drag and under-predicts lift, this is due to shockwave formations not fully captured. Another area of concern is where separation is present, such as around the nacelles in the NASA X-57. With those areas of improvement highlighted, we showed SUAVE's Fidelity Zero performed nearly equivalently to panel codes for supersonic flight and showed excellent agreement with CFD, it also showed excellent agreement in cases without separation, and showed nearly identical results to Athena Vortex Lattice for control surface deflections.

Assuring that conceptual level design trade offs are captured by these analyses at attractive computational speed is essential. By performing these verification and validation cases, we have demonstrated SUAVE's applicability to a wide range of scenarios. This work intends to lay the ground work for future work in SUAVE to continue improving analyses, while staying within the scope of conceptual level analyses. Confident in these basic analyses, the development of SUAVE turns to exploiting these aerodynamic capabilities for new methods of aerospace design.

References

[1] Lukaczyk, T. W., Wendorff, A. D., Colonno, M., Economon, T. D., Alonso, J. J., Orra, T. H., and Ilario, C., "SUAVE: an open-source environment for multi-fidelity conceptual vehicle design," *16th AIAA/ISSMO Multidisciplinary Analysis and Optimization Conference*, 2015, p. 3087.

[2] MacDonald, T., Botero, E., Vegh, J. M., Variyar, A., Alonso, J. J., Orra, T. H., and Ilario da Silva, C. R., "SUAVE: An Open-Source Environment Enabling Unconventional Vehicle Designs through Higher Fidelity," *55th AIAA Aerospace sciences meeting*, 2017, p. 0234.

[3] MacDonald, T., Clarke, M., Botero, E. M., Vegh, J. M., and Alonso, J. J., "SUAVE: an open-source environment enabling multi-fidelity vehicle optimization," *18th AIAA/ISSMO Multidisciplinary Analysis and Optimization Conference*, 2017, p. 4437.

[4] Owens, D., "Weissinger's Model of the Nonlinear Lifting-Line Method for Aircraft Design," *36th AIAA Aerospace Sciences Meeting and Exhibit*, 1998, p. 597.

[5] Miranda, L. R., Elliot, R. D., and Baker, W. M., "A Generalized Vortex Lattice Method for Subsonic and Supersonic Flow Applications," *NASA Technical Report*, 1977.

[6] Botero, E., Clarke, M., MacDonald, T., jmvegh, Lukaczyk, T., Erhard, R., da Silva, C. R. I., tmomose, AaronBlau, Smart, J., tarikorra, awendorff, Maier, W., Gonçalves, P., stankarpuk93, tstfrancis, cmcmillan8, Bianchi, D., wvangijseghem, anilvar, Mukhopadhaya, J., fcapristan, bdalman, stankarpuktubs, and Kruger, M., "suavecode/SUAVE: SUAVE 2.5.0," , Nov. 2021. https://doi.org/10.5281/zenodo.5661107, URL https://doi.org/10.5281/zenodo.5661107.

[7] Vassberg, J., Dehaan, M., Rivers, M., and Wahls, R., "Development of a Common Research Model for Applied CFD Validation Studies," *26th AIAA applied aerodynamics conference*, 2008, p. 6919.

[8] Vassberg, J. C., DeHaan, M. A., Rivers, M. S., and Wahls, R. A., "Retrospective on the Common Research Model for Computational Fluid Dynamics Validation Studies," *Journal of Aircraft*, Vol. 55, No. 4, 2018, pp. 1325–1337.

[9] Rivers, M., Hunter, C., and Campbell, R., "Further investigation of the support system effects and wing twist on the NASA common research model," *30th AIAA Applied Aerodynamics Conference*, 2012, p. 3209.

[10] Tinoco, E. N., Brodersen, O. P., Keye, S., Laflin, K. R., Feltrop, E., Vassberg, J. C., Mani, M., Rider, B., Wahls, R. A., Morrison, J. H., et al., "Summary data from the sixth AIAA CFD drag prediction workshop: CRM cases," *Journal of Aircraft*, Vol. 55, No. 4, 2018, pp. 1352–1379.

[11] Rivers, M., and Dittberner, A., "Experimental investigations of the nasa common research model in the nasa langley national transonic facility and nasa ames 11-ft transonic wind tunnel," *49th AIAA aerospace sciences meeting including the new horizons forum and aerospace exposition*, 2011, p. 1126.

[12] Nicolosi, F., Della Vecchia, P., and Corcione, S., "Design and aerodynamic analysis of a twin-engine commuter aircraft," *Aerospace Science and Technology*, Vol. 40, 2015, pp. 1–16. https://doi.org/10.1016/j.ast.2014.10.008.

[13] Yoo, S., and Duensing, J., "Computational Analysis of the External Aerodynamics of the Unpowered X-57 Mod-III Aircraft," , No. June, 2019, pp. 1–18. https://doi.org/10.2514/6.2019-3698.

[14] Carmichael, R., and Erickson, L., "PAN AIR-A higher order panel method for predicting subsonic or supersonic linear potential flows about arbitrary configurations," *14th Fluid and Plasma Dynamics Conference*, 1981, p. 1255.

[15] Palacios, F., Colonno, M. R., Aranake, A. C., Campos, A., Copeland, S. R., Economon, T. D., Lonka, A. K., Lukaczyk, T. W., Taylor, T. W. R., and Alonso, J. J., "Stanford University Unstructured (SU2): An open-source integrated computational environment for multi-physics simulation and design," *51st AIAA Aerospace Sciences Meeting and Exhibit*, Grapevine, TX, 2013.

[16] Raymer, D. P., "Aircraft design: a conceptual approach (AIAA Education Series)," *Reston, Virginia*, 2012.

[17] Drela, M., and Youngren, H., "AVL," http://web.mit.edu/drela/Public/web/avl/, May 2017.

[18] Veldhuis, L. L. M., "Propeller Wing Aerodynamic Interference," Ph.D. thesis, 2005.

[19] Clarke, M. A., Erhard, R. M., and Alonso, J., "Aerodynamic Optimization of Wing-Mounted Propeller Configurations for Distributed Electric Propulsion Architectures," 2021, pp. 1–19. https://doi.org/10.2514/6.2021-2471.

[20] Schmitt, V., and Charpin, F., "Pressure Distributions on the ONERA-M6-Wing at Transonic Mach Numbers," *Experimental Data Base for Computer Program Assessment. Report of the Fluid Dynamics Panel Working Group 04, AGARD AR 138*, 1979.

[21] "Onera M6 Wing," , Feb 2021. URL https://www.grc.nasa.gov/www/wind/valid/m6wing/m6wing.html.